Available online at www.sciencedirect.com
ScienceDirect
International Journal of Heat and Mass Transfer 51 (2008) 2199–2213
International Journal of HEAT and MASS TRANSFER
www.elsevier.com/locate/ijhmt

Flow and heat transfer characteristics of the boundary layers over a stretching surface with a uniform-shear free stream

Tiegang Fang *

Mechanical and Aerospace Engineering Department, North Carolina State University, 3182 Broughton Hall – Campus Box 7910, 2601 Stinson Drive, Raleigh, NC 27695, USA

Received 23 July 2007; received in revised form 1 November 2007
Available online 31 December 2007

Abstract

In this work, the momentum and thermal boundary layers over a continuously stretching surface with a uniform-shear free stream were investigated. Based on the boundary layer assumptions, the similarity equations were obtained, which were solved numerically. Theoretical analysis was conducted for certain special conditions. The solution domain for the momentum boundary layer was theoretically estimated and compared with the numerical results. It is found that the interaction of uniform-shear free stream and the wall stretching velocity greatly affects the fluid motion and heat transfer characteristics. Dual solutions exist for the stretching parameter $\gamma > \gamma_c = -0.596985$. There is one solution for $\gamma = \gamma_c$ and no solution for $\gamma < \gamma_c$. The effects of the Prandtl number, Pr, the temperature power index, m, and the wall stretching parameter, γ, on the heat transfer behaviors were analyzed and discussed. A general exact analytical solution of thermal boundary layers was derived for non-stretching wall condition with $\gamma = 0$ and arbitrary values of Pr and γ. Analytical solutions were also given for $m = -\frac{2}{3}$ and $m = 0$ with arbitrary values of Pr and m. Interesting observations were found for negative wall stretching parameter, negative temperature power index, and the lower solution branch.

Keywords: Similarity solution; Stretching surface; Power-law shear flow; Uniform-shear free stream

1. Introduction

The boundary layer flow over a continuously stretching surface is an often-encountered problem in many engineering processes. There are lots of applications in industries such as the hot rolling, wire drawing, glass–fiber production, etc. [1–3]. In these processes, it is very important to control the drag and the heat flux at the stretching surface in order to obtain good product quality.

The pioneering work in this area was conducted by Sakiadis [4,5]. Sakiadis analyzed the boundary layer assumptions and the governing equations of the problem, and the boundary layer flow on a continuously stretching surface with a constant speed was investigated. His work was further verified by Tsou et al. [6] experimentally. The thermal boundary layer with a constant wall temperature was also discussed [6]. Following these works, the boundary conditions on the surface were generalized by other researchers [7–12]. The velocity of the surface was extended to be a function of distance from the slot, where the surface was stretched out. A power-law function was the most common case. Thermal boundary conditions included a power-law surface temperature or a power-law surface heat flux. Mass transfer such as fluid suction and injection was also considered on the stretching surface. The boundary layers over a stretching surface with a parallel constant velocity free stream were investigated [13–15]. The interaction of free-stream velocity and wall stretching speed greatly changed the momentum and heat transport in the boundary layers.

In recent years, a bulk of studies in power-law shear driven boundary layer flows were published in various journals [16–26]. An early work of the boundary layers with

* Tel.: +1 919 5155230.
E-mail address: tfang2@ncsu.edu

0017-9310/$ - see front matter © 2007 Elsevier Ltd. All rights reserved.
doi:10.1016/j.ijheatmasstransfer.2007.11.013

Nomenclature

f	dimensionless free-stream function
f'	first derivative of f
f''	second derivative of f
f'''	third derivative of f
f''''	fourth derivative of f
g	dimensionless temperature
g'	first derivative of g
g''	second derivative of g
m	power exponent for the wall temperature distribution
q_w	wall heat flux
t	dummy variable
u	fluid velocity in x direction
v	fluid velocity in y direction
x	coordinate along the free-stream direction
y	coordinate perpendicular to the free-stream direction
z	defined new variable
L	characteristic length of the current flow configuration
Pr	Prandtl number
T	fluid temperature
T_w	surface temperature
T_r	reference temperature
T_∞	free-stream fluid temperature
U_i	induced free-stream velocity due to wall stretching
U_w	surface stretching velocity
U_∞	free-stream velocity
Z	defined new variable

Greek symbols

α	thermal diffusivity
β	uniform-shear strength
δ	dimensionless wall stress, $f'(0)$
ϵ	dummy variable
η	similarity variable
γ	wall stretching parameter
ν	kinematic viscosity
Ψ	stream function
Γ	gamma function

a shear flow free stream was published by Wang to study the mixing layers driven by a shear flow [16]. This work was further generalized to a power-law shear driven free-stream flow [17]. With a shear flow in the free stream, the free stream is no longer rotation-free. It was found that the flow motion and momentum transport behaviors were quite different from a rotation-free flow [17]. The power-law shear driven flow with mass transfer at the wall was studied for some velocity power indices [18]. Solution domain and the boundary layer characteristics of different power indices were discussed [19,20]. Power series solution was presented through the application of some analytical techniques and the convergence characteristics were analyzed for the momentum and thermal boundary layers [21]. The heat transfer characteristics were also investigated for different power indices and some analytical solutions were presented [19,21–26]. Analytical solutions for the special cases for a power index of $-1/2$ with an adiabatic wall were presented and discussed [22]. Magyari and Weidman reported the exact solutions for the boundary layers of an Airy wall jet with preheating [23] or constant wall heat flux [24]. The thermal boundary layer with a uniform-shear free stream was studied and compared with the famous Blasius flow [25]. It was shown that the dependence of the wall heat flux on the Prandtl numbers were quite different for both flow configurations. More analytical solutions were given in an earlier paper by Wang for the heat transfer problem of a Couette shear free stream [26]. However, in most of the works, the flat surface was kept stationary with no wall stretching. The interaction of free stream and wall stretching greatly affects the momentum and heat transport in the boundary layer over the surface. As mentioned by Wang [16] when there was a fluid velocity at the mixing layer interface, the free stream was no longer a pure Couette flow profiles but with an induced fluid velocity at large distance from the interface. The objective of this work is to study the influence of uniform-shear flow on the boundary layers over a stretching surface. Similarity equations of the boundary layers over a stretching surface are obtained and solved numerically. Influences of various parameters on the boundary layers are discussed.

2. Mathematical formulation

Consider a steady, two-dimensional laminar flow over a continuously stretching surface in the presence of a free stream with uniform shear $\frac{dU_\infty}{dy} = \beta$. The wall stretching velocity is $U_w = U_w(x)$ and the wall temperature is $T_w = T_w(x)$ with an ambient temperature T_∞. This uniform-shear flow includes both the classical Couette flow profiles, namely $U_\infty = \beta y$, and linear flow of y with a certain induced fluid velocity due to wall stretching, say $U_\infty = \beta y + c(x)$. Based on the later discussion, it is shown that $c(x) \propto x^{\frac{1}{3}}$. The x-axis runs along the stretching surface in the direction of the motion and the y-axis is perpendicular to it. Based on boundary layer assumptions [16,27], the governing equations of this problem become

$$\frac{\partial u}{\partial x} + \frac{\partial v}{\partial y} = 0, \tag{1}$$

$$u\frac{\partial u}{\partial x}+v\frac{\partial u}{\partial y}=v\frac{\partial^2 u}{\partial y^2}, \tag{2}$$

$$u\frac{\partial T}{\partial x}+v\frac{\partial T}{\partial y}=\alpha\frac{\partial^2 T}{\partial x^2} \tag{3}$$

with the boundary conditions

$$u(x,0)=U_w(x),\quad v(x,0)=0,\quad \frac{\partial u(x,\infty)}{\partial y}=\beta,$$
$$T(x,0)=T_w(x),\quad T(x,\infty)=T_\infty, \tag{4}$$

where u and v are the velocity components in the x and y directions respectively, v is the kinematic viscosity, α is the thermal diffusivity and T is the fluid temperature. The problem can be rescaled with a characteristics length $L=\sqrt{\frac{v}{\beta}}$. The stream function, similarity variable, and temperature profiles can be posited in the following form [25]:

$$\Psi(x,y)=v\left(\frac{x}{L}\right)^{\frac{2}{3}}f(\eta), \tag{5a}$$

$$T(x,y)=T_\infty+T_r\left(\frac{x}{L}\right)^m g(\eta), \tag{5b}$$

$$\eta=\left(\frac{x}{L}\right)^{-\frac{1}{3}}\frac{y}{L}, \tag{5c}$$

where T_r is a reference temperature. With these definitions, the velocities are expressed as $u=vL^{-\frac{4}{3}}x^{\frac{1}{3}}f'(\eta)$ and $v=\frac{1}{3}vL^{-\frac{2}{3}}x^{-\frac{1}{3}}[f'(\eta)\eta-2f(\eta)]$. Therefore, the similarity equations are obtained as follows:

$$3f'''+2ff''-f'^2=0, \tag{6}$$

$$\frac{3}{Pr}g''+2fg'-3mf'g=0 \tag{7}$$

with boundary conditions (BCs)

$$f(0)=0,\quad f'(0)=\gamma,\quad f''(\infty)=1,\quad g(0)=1,$$
$$\text{and}\quad g(\infty)=0. \tag{8a–e}$$

The wall stretching velocity is $U_w(x)=vL^{-\frac{4}{3}}x^{\frac{1}{3}}\gamma\propto x^{\frac{1}{3}}$, and γ is the wall stretching parameter. Here γ can be either a positive number or a negative number. For a positive value of γ, the boundary layer is the commonly encountered forward boundary layer as discussed by many researcher in the literature. However, for a negative value of γ, the boundary layer belongs to the so-called backward boundary layer [28] as discussed by Goldstein. For a backward boundary layer, namely the surface moving from $+\infty$ to the slot, the fluid loses any memory of the perturbation introduced by the leading edge, say the slot. Therefore, for different wall stretching parameters, the two different boundary layers show quite distinct physical phenomena. The wall temperature has a power-law distribution with the distance from the origin. Based on the derivation, it is known that similarity equations only exist for a 1/3-power wall stretching velocity and a power-law wall temperature. Since there is no general analytic solutions for the similarity equations, Eqs. (6) and (7) combined with the boundary conditions (8a–e) were solved by using the so-called shooting method [27] to convert the boundary value problem to an initial value problem. A fourth-order Runge–Kutta integration scheme was adopted to solve the applicable initial value problem [27].

3. Results and discussion

3.1. Momentum boundary layer

The momentum boundary layer equation can be further analyzed by differentiating Eq. (6) as follows:

$$3f''''+2ff''''=0 \tag{9}$$

with BCs

$$f(0)=0,\quad f'(0)=\gamma,\quad f''(\infty)=1,\quad f'''(0)=\frac{\gamma^2}{3}. \tag{10a–d}$$

Eq. (9) can be integrated twice as

$$f''(\eta)=\frac{\gamma^2}{3}\int_0^\eta e^{-\frac{2}{3}\int_0^t f(\epsilon)d\epsilon}dt+\delta, \tag{11}$$

where $\delta=f''(0)$. Evaluating $f''(\infty)$ yields

$$\frac{\gamma^2}{3}\int_0^\infty e^{-\frac{2}{3}\int_0^t f(\epsilon)d\epsilon}dt+\delta=1\leftrightarrow\delta$$
$$=1-\frac{\gamma^2}{3}\int_0^\infty e^{-\frac{2}{3}\int_0^t f(\epsilon)d\epsilon}dt. \tag{12}$$

Based on the physical configuration, it is expected that for positive stretching, $\gamma>0, f(\eta)>\frac{1}{2}\eta^2$, and for negative stretching, $\gamma<0, f(\eta)<\frac{1}{2}\eta^2$. However, as will be discussed in the numerical solutions, this analysis is only valid for the upper solution branch. Substituting these conditions into Eq. (12) yields for $\gamma>0$

$$\delta>1-\frac{\gamma^2}{3}\int_0^\infty e^{-\frac{\eta^3}{9}}d\eta=1-\frac{\Gamma\left(\frac{1}{3}\right)\gamma^2}{3\sqrt[3]{3}}$$
$$=1-0.619157\gamma^2 \tag{13}$$

and for $\gamma<0$

$$\delta<1-\frac{\gamma^2}{3}\int_0^\infty e^{-\frac{\eta^3}{9}}d\eta=1-\frac{\Gamma\left(\frac{1}{3}\right)\gamma^2}{3\sqrt[3]{3}}. \tag{14}$$

From Eq. (11), it is seen that $f''(\eta)$ is a monotonously increasing function of η and $f''(\eta)\in[\delta,1]$. Then it is obtained $\delta\eta+\gamma<f'(\eta)<\eta+\gamma$, which yields

$$\frac{\delta\eta^2}{2}+\gamma\eta<f(\eta)<\frac{\eta^2}{2}+\gamma\eta. \tag{15}$$

Plugging Eq. (15) into (12) yields

$$1-\frac{\gamma^2}{3}\int_0^\infty e^{-\frac{\eta^3}{9}-\frac{\gamma\eta^2}{3}}dt>\delta>1-\frac{\gamma^2}{3}\int_0^\infty e^{-\frac{\delta\eta^3}{9}-\frac{\gamma\eta^2}{3}}dt. \tag{16}$$

From the left-hand side of Eq. (16) one obtains for $\gamma>0, \int_0^\infty e^{-\frac{\eta^3}{9}-\frac{\gamma\eta^2}{3}}dt<\frac{\Gamma\left(\frac{1}{3}\right)}{\sqrt[3]{3}}$. However for $\gamma<0$, there are some interesting results. Based on the left-hand side of Eq. (16), a function $h(\gamma)$ can be obtained as

$$h(\gamma) = 1 - \frac{\gamma^2}{3}\int_0^\infty e^{-\frac{\eta^3}{9}-\frac{\gamma\eta^2}{3}}dt. \tag{17}$$

The right-hand side of Eq. (16) generates another function in implicit form

$$1 - \frac{\gamma^2}{3}\int_0^\infty e^{-\frac{\delta\eta^3}{9}-\frac{\gamma\eta^2}{3}}dt - \delta = 0 \leftrightarrow \delta = p(\gamma). \tag{18}$$

Eqs. (17) and (18) provide much better estimation of the solution domain as shown in a later section compared with the numerical solutions. However, it should be noticed that Eq. (18) is only valid for $\delta \geqslant 0$ due to the definite integral in the equation.

By using a new variable transformation $f(\eta) = \sqrt{\gamma}F(\sqrt{\gamma}\eta) = \sqrt{\gamma}F(z)$, it is obtained

$$3F'''' + 2FF'''' = 0 \tag{19}$$

with boundary conditions

$$F(0) = 0, \quad F'(0) = 1, \quad F''(\infty) = \frac{1}{\sqrt{\gamma^3}}, \quad F'''(0) = \frac{1}{3}. \tag{20a–d}$$

The prime denotes differentiation with respect to z. Eq. (19) is valid for any valve of γ. For a very large value of γ, $F''(\infty) = 0$. By numerical integration, it is obtained $F''(0) = -0.677648$. Therefore, for very large γ, $f''(0) = -0.677648\gamma^{1.5}$.

Since there is no general analytical solution for the similarity equations, numerical technique has to be used to solve the boundary value problems. The fourth order Runge–Kutta integration scheme was used in the shooting technique [27]. The code was validated using the previous reported values from references [16,25]. During the computation, the shooting error was controlled less than 10^{-6}. The momentum boundary layer equation was solved first and followed by the thermal boundary layer. The solution domain for Eq. (6) with BCs ((8a–c)) is illustrated in Fig. 1. It is seen that the solution only exists for a certain range of wall stretching parameter γ. There is a critical wall stretching parameter, $\gamma_c = -0.596985$. When $\gamma < \gamma_c$, there is no solution. When $\gamma = \gamma_c$, there is only one solution. There are dual solutions for $\gamma > \gamma_c$. Some typical values of $f''(0)$ for different values of the wall stretching parameter are tabulated in Table 1 for the two solution branches. For a small wall stretching parameter with $|\gamma|$ close to zero, the wall-shear stress becomes less with either positive or negative stretching compared with the non-stretching wall condition. As shown in Fig. 2, a closer look at the negative wall stretching solution domain indicates that when $-0.30015 < \gamma < 0$, the wall-shear stress becomes negative showing more reversal flow for the lower solution branch. The wall-shear stress becomes zero when $\gamma = -0.30015$ or $\gamma = 1.61091$, and the latter was first discussed by Wang [16]. The estimated solution domains are also shown in Fig. 2. Eq. (16) does give a better estimation than Eqs. (13) and (14). Especially for Eq. (18), it closely follows the real solution domain and also provides a good estimation for the dual solution domain. For a positive γ, $f''(0)$ decreases with the increase of γ for both solution branches. As discussed above, for a very large γ, $f''(0) \rightarrow -0.677648\gamma^{1.5}$. Another interesting result is that with wall stretching, the free-stream velocity is no longer a pure Couette shear flow profile. There is an induced velocity due to the wall movement, which was noticed by Wang [16]. The non-dimensional induced velocity can be expressed by $U_i = \lim_{\eta\to\infty} f'(\eta) - \eta$, which is shown in Fig. 3. It is seen

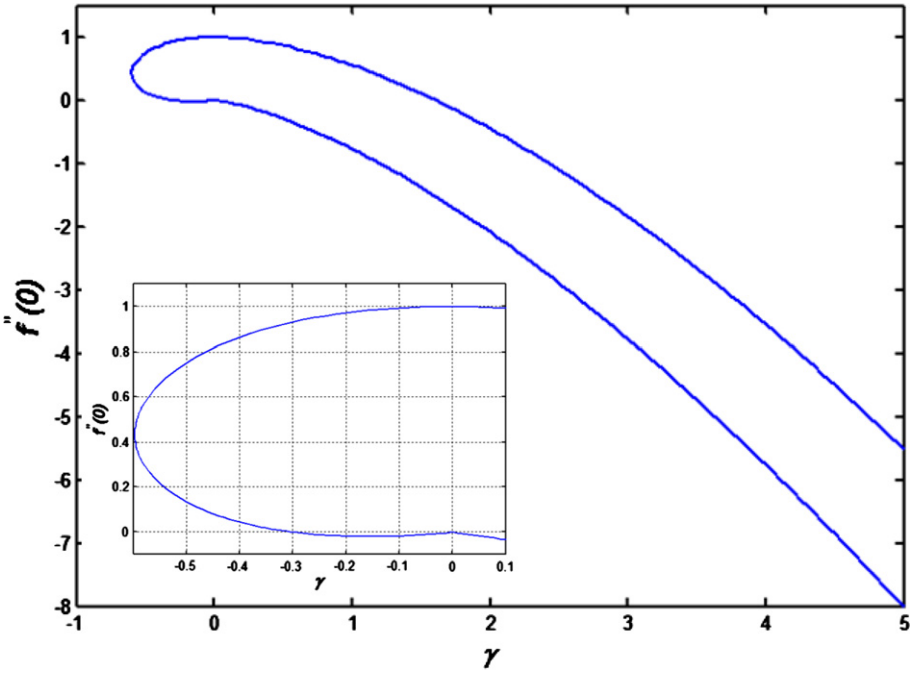

Fig. 1. The solution domain for the momentum boundary layer equation.

Table 1
Typical values of $f''(0)$ at different wall stretching parameters for the two solution branches

γ	$f''(0)$ lower branch	$f''(0)$ upper branch	γ	$f''(0)$ lower branch	$f''(0)$ upper branch	γ	$f''(0)$ lower branch	$f''(0)$ upper branch
5.0	−8.012006	−5.512634	2.0	−2.084092	−0.443590	−0.1	−0.017703	0.993440
4.5	−6.857851	−4.495868	1.5	−1.370725	0.114963	−0.2	−0.018388	0.971925
4.0	−5.764323	−3.541548	1.0	−0.762885	0.562553	−0.3	−0.000045	0.931424
3.5	−4.735123	−2.653668	0.5	−0.285126	0.874245	−0.4	0.044824	0.864452
3.0	−3.774719	−1.837069	0.2	−0.082120	0.977493	−0.5	0.134657	0.752585
2.5	−2.888659	−1.097782	0.1	−0.034376	0.994114	−0.59	0.345647	0.521823

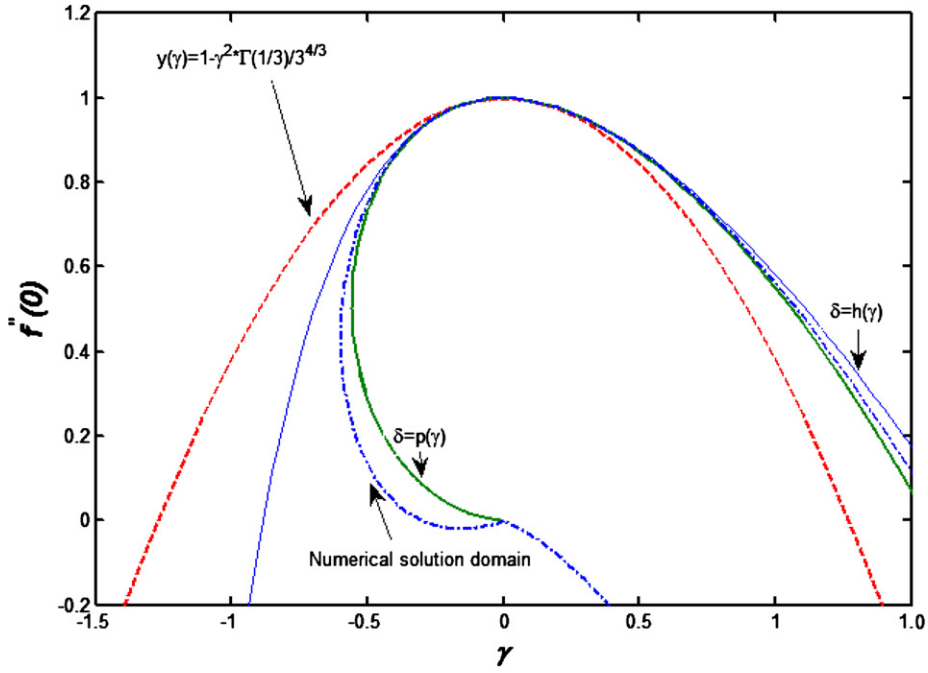

Fig. 2. Comparison of the numerical solution domain and theoretical estimation.

that positive wall stretching leads to a positive induced velocity for the upper solution branch and negative stretching and lower solution branch result in a negative induced velocity. This argument has been used in the derivation of Eqs. (13) and (14). However, this induced flow is overwhelmed by the free stream at large distance from the wall. Interesting observation is found for negative wall stretching and the lower solution branch for positive stretching. The induced velocity becomes more negative with the transition from the upper solution branch to the lower solution branch. It is expected that $U_i \to -\infty$ when $\gamma \to -0$ for the lower solution branch. This induced flow is similar to the mass suction or mass blowing at the wall. For a positive induced velocity, the velocity profile is somehow sucked to the wall, while for a negative one, the velocity profile is blown away from the wall, which has similar effects to the moving-wall boundary layer [29–32]. For the condition with $U_i \to -\infty$, the velocity profile is similar to a hard blowing problem and is located much further away from the wall with near zero wall stress. For the lower solution branch of positive stretching, as the stretching parameter increases, the induced fluid velocity gradually increases from $-\infty$ to a certain negative value.

In order to further understand the effects of the wall stretching parameter on the momentum boundary layers, some examples of the velocity profiles are illustrated in Figs. 4 and 5. As shown in Fig. 4 for negative wall movement, the velocity profiles move further away from the wall, which has a similar effect to the mass blowing at the wall compared with the Couette flow profile plotted in the same figure. Two solutions for $\gamma = -0.4$ are also shown in the plots. Compared with the upper branch, the wall stress becomes much less and the velocity profile becomes much further away from the wall for the lower solution branch. The lower solution branch is very different from the upper solution branch. For negative stretching parameter, there is always a reversal flow. Velocity profiles for a positive stretching parameter are shown in Fig. 5. For a large positive wall stretching parameter, i.e. $\gamma = 3.0$, the fluid near the wall is dragged by the wall not by the free-stream shear. There is a region between the wall and the free stream with a minimum fluid velocity. Due to positive wall stretching, the velocity profiles are drawn closer to the wall like a certain kind of flow suction. For a positive stretching parameter, the lower solution branch also shows some reversal flow as seen in Fig. 5. The physical meaning

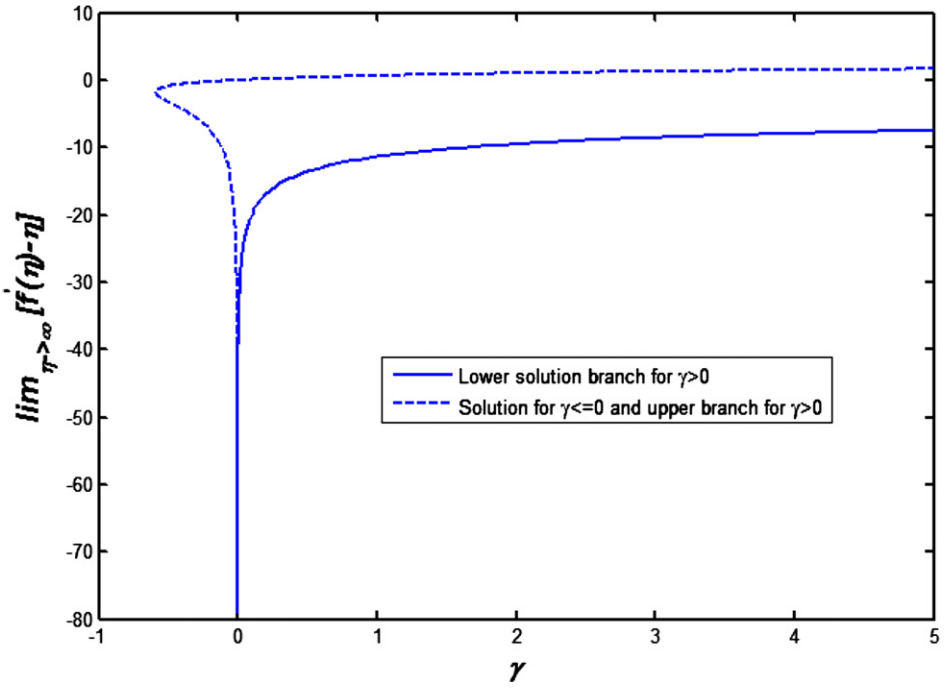

Fig. 3. The induced free-stream velocity for different wall stretching parameter.

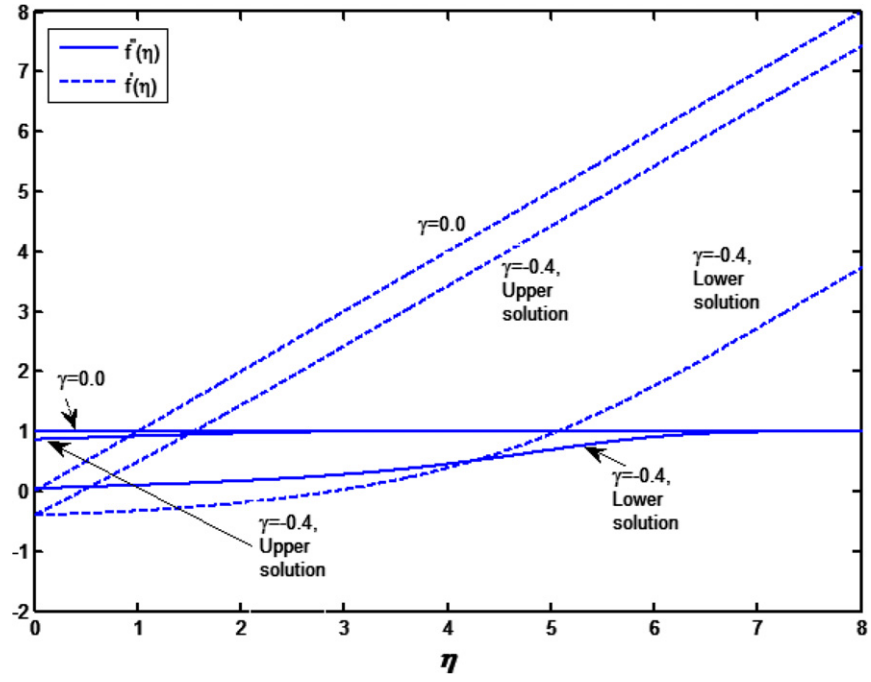

Fig. 4. Examples of the velocity and shear stress profiles for $\gamma = 0$ and $\gamma = -0.4$.

of the lower solution branch is worthy of further investigation. The wall-shear-free velocity profiles are shown in Fig. 6. Compared with the large wall stretching conditions, the minimum velocity occurs on the wall and monotonously increases with the increase of the distance from the wall.

3.2. Thermal boundary layer

The thermal boundary layer equation is a linear second-order ordinary differential equation (ODE). Under certain conditions, analytical solutions can be obtained as shown below.

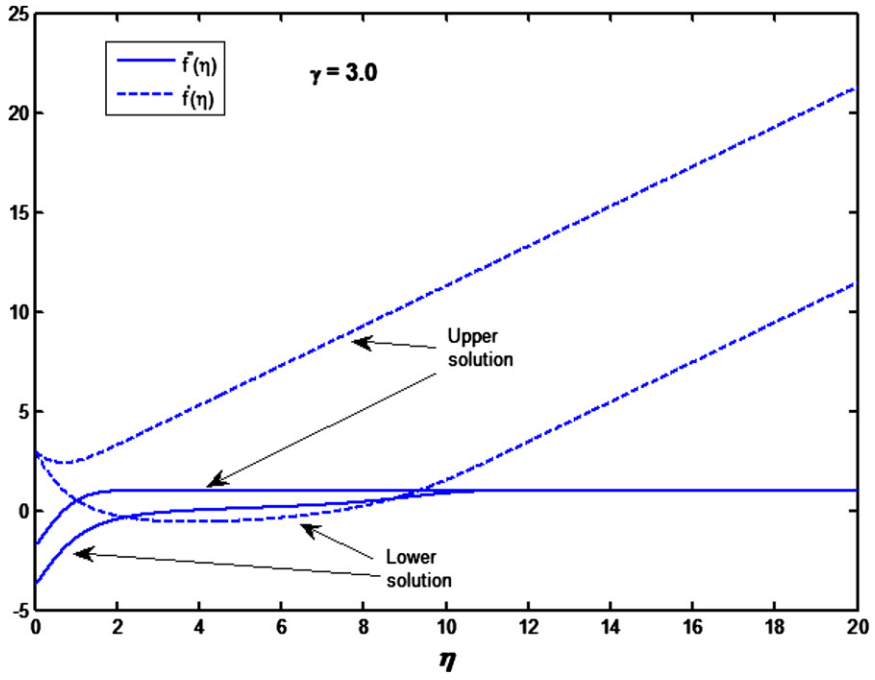

Fig. 5. Examples of the velocity and shear stress profiles for $\gamma = 3.0$.

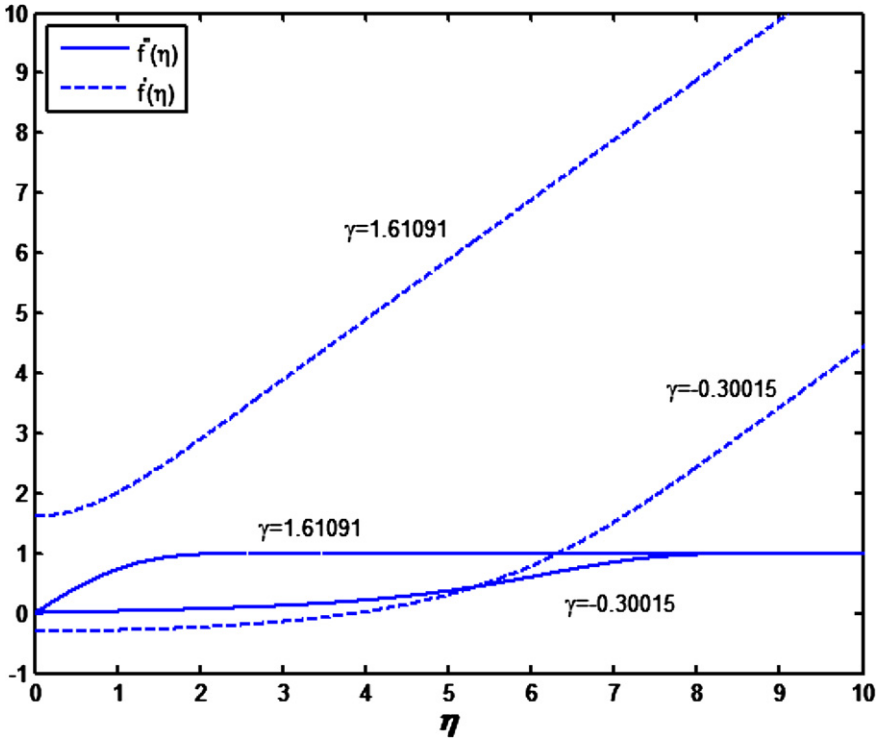

Fig. 6. The velocity and shear stress profiles for shear-free wall stretching parameters.

3.2.1. Analytical solution for $m = -2/3$ and $m = 0$

When $m = -2/3$, Eq. (7) becomes

$$\frac{3}{Pr}g'' + 2fg' + 2f'g = 0. \tag{21}$$

The solution reads

$$g(\eta) = Ce^{-\frac{2Pr}{3}\int_0^\eta f(t)\mathrm{d}t} + g'(0)e^{-\frac{2Pr}{3}\int_0^\eta f(t)\mathrm{d}t}\int_0^\eta e^{\frac{2Pr}{3}\int_0^t f(\epsilon)\mathrm{d}\epsilon}\mathrm{d}t. \tag{22}$$

Based on the boundary conditions, it is obtained

$$g(\eta)=\mathrm{e}^{-\frac{2Pr}{3}\int_0^\eta f(t)\mathrm{d}t}\left(1-\frac{\int_0^\eta \mathrm{e}^{\frac{2Pr}{3}\int_0^t f(\epsilon)\mathrm{d}\epsilon}\mathrm{d}t}{\int_0^\infty \mathrm{e}^{\frac{2Pr}{3}\int_0^t f(\epsilon)\mathrm{d}\epsilon}\mathrm{d}t}\right). \tag{23}$$

Because $\int_0^\infty \mathrm{e}^{\frac{2Pr}{3}\int_0^t f(\epsilon)\mathrm{d}\epsilon}\mathrm{d}t\to\infty$, the solution becomes

$$g(\eta)=\mathrm{e}^{-\frac{2Pr}{3}\int_0^\eta f(t)\mathrm{d}t}. \tag{24}$$

The wall heat flux is $q_w=\frac{kT_r}{L}\left(\frac{x}{L}\right)^{m-\frac{1}{3}}g'(0)$. For this case, the wall becomes adiabatic with no heat transfer. This case corresponds to a special situation with a heating source at the leading edge and the total heat energy is conserved in the fluid as it flows along the wall.

Another case is for $m=0$, the solution becomes

$$g(\eta)=1-\frac{\int_0^\eta \mathrm{e}^{-\frac{2Pr}{3}\int_0^t f(\epsilon)\mathrm{d}\epsilon}\mathrm{d}t}{\int_0^\infty \mathrm{e}^{-\frac{2Pr}{3}\int_0^t f(\epsilon)\mathrm{d}\epsilon}\mathrm{d}t}. \tag{25}$$

The non-dimensional wall heat flux is

$$g'(0)=-\frac{1}{\int_0^\infty \mathrm{e}^{-\frac{2Pr}{3}\int_0^t f(\epsilon)\mathrm{d}\epsilon}\mathrm{d}t}. \tag{26}$$

3.2.2. Exact solution for $\gamma=0$ and arbitrary m

When there is no stretching on the surface, Eq. (7) becomes

$$\frac{3}{Pr}g''+\eta^2 g'-3m\eta g=0. \tag{27}$$

Using an new variable as $z=\sqrt[3]{Pr}\eta$ yields

$$g''+\frac{z^2}{3}g'-mzg=0. \tag{28}$$

There is an analytical solution for the above equation for non-zero m as

$$g(\eta)=\Phi\left(-m,\frac{2}{3},-\frac{Pr\eta^3}{9}\right)-3^{\frac{4}{3}}\times\frac{\Gamma\left(\frac{2}{3}\right)\Gamma(1+m)}{\Gamma\left(\frac{4}{3}\right)\Gamma\left(\frac{2}{3}+m\right)}\eta\Phi\left(\frac{1}{3}-m,\frac{4}{3},-\frac{Pr\eta^3}{9}\right), \tag{29}$$

where $\Phi(a,b,x)$ is the confluent hypergeometric function or the first kind of Kummer function [33], and $\Gamma(x)$ is the Gamma function. The wall heat flux becomes

$$-g'(0)=3^{-\frac{2}{3}}\frac{\Gamma\left(\frac{2}{3}\right)\Gamma(1+m)}{\Gamma\left(\frac{4}{3}\right)\Gamma\left(\frac{2}{3}+m\right)}Pr^{\frac{1}{3}}. \tag{30}$$

Based on the properties of the Gamma function, when x is a non-positive integer number, $|\Gamma(x)|\to\infty$. Therefore, it is concluded that the wall becomes adiabatic for $m+\frac{2}{3}=0,-1,-2,-3,\ldots$, and there is no finite solution when $m+1=0,-1,-2,-3,\ldots$. These findings generalize the previous results [25,26]. A limiting situation is for $Pr\to\infty$, in this case, the thermal boundary layer is very thin compared with the momentum boundary layer Eq. (7) can be approximated as

$$\frac{3}{Pr}g''+2\gamma\eta g'-3m\gamma g=0. \tag{31}$$

With a new variable $Z=\eta\sqrt{Pr|\gamma|}$, it is obtained for $\gamma>0$

$$g''+\frac{2}{3}\eta g'-mg=0. \tag{32}$$

And for $\gamma<0$

$$g''-\frac{2}{3}\eta g'+mg=0. \tag{33}$$

The solution reads for $\gamma>0$

$$g(Z)=\frac{\mathrm{e}^{-\frac{Z^2}{3}}Z\Gamma\left(1+\frac{3m}{4}\right)U\left(1+\frac{3m}{4},\frac{3}{2},\frac{Z^2}{3}\right)}{\sqrt{3\pi}}, \tag{34}$$

where $U(1+\frac{3m}{4},\frac{3}{2},\frac{Z^2}{3})$ is the second kind of Kummer function [33]. Consequently, the wall heat flux becomes

$$-g(0)=\frac{2}{\sqrt{3}}\frac{\Gamma\left(1+\frac{3m}{4}\right)}{\Gamma\left(\frac{1}{2}+\frac{3m}{4}\right)}\sqrt{Pr\gamma},\ \gamma>0. \tag{35}$$

There is no solution for Eq. (33) satisfying the boundary conditions. For example, for $m=0$, solution of Eq. (33) is $g(Z)=A\mathrm{e}^{\frac{Z^2}{3}}$, which does not satisfy the boundary at $Z\to\infty$. Another example is for $m=-\frac{2}{3}$. The solution reads $g(Z)=\mathrm{e}^{\frac{Z^2}{3}}[1+g'(0)\int_0^Z \mathrm{e}^{-\frac{t^2}{3}}\mathrm{d}t]$ and it is obvious that the boundary condition is not satisfied at $Z\to\infty$. These results are based on the approximated Eq. (31) and do not mean that there is no solution for negative γ for a large Prandtl number. It does show that this approximation is not applicable for a negative γ.

As we discussed before, when Pr is very large, there are some approximated solutions of the boundary layers as shown by Eq. (34). For non-negative stretching velocity and positive m, when m is large enough, Eq. (34) is also applicable. From Eq. (35), based on the series expansion of the Gamma function for large m, it is obtained that

$$-g'(0)=\frac{2}{\sqrt{3}}\frac{\Gamma\left(1+\frac{3m}{4}\right)}{\Gamma\left(\frac{1}{2}+\frac{3m}{4}\right)}\sqrt{Pr\gamma}\to\lim_{m\to\infty}-g'(0)=\sqrt{mPr\gamma}. \tag{36}$$

When $\gamma=0$, from Eq. (30), one obtains for very large m,

$$-g'(0)=3^{-\frac{2}{3}}\frac{\Gamma\left(\frac{2}{3}\right)\Gamma(1+m)}{\Gamma\left(\frac{4}{3}\right)\Gamma\left(\frac{2}{3}+m\right)}Pr^{\frac{1}{3}}\to\lim_{m\to\infty}-g'(0)=3^{-\frac{2}{3}}\frac{\Gamma\left(\frac{2}{3}\right)}{\Gamma\left(\frac{4}{3}\right)}(mPr)^{\frac{1}{3}}. \tag{37}$$

3.2.3. Numerical solution of the thermal boundary layers

3.2.3.1. Upper solution branch for $\gamma\geqslant 0$. With more parameters involved in the thermal boundary layers, the variation behaviors become quite complicated. Some temperature profiles for different stretching parameters and temperature power indices m are shown in Fig. 7 with $Pr=0.7$. For positive wall stretching, the thermal boundary layers are closer to the wall compared with the non-moving-wall case. With the increase of m, the thermal boundary layers become thinner. The wall heat fluxes increase with the increase of m and γ for non-negative m. However, for negative m, the maximum temperature gradient occurs in

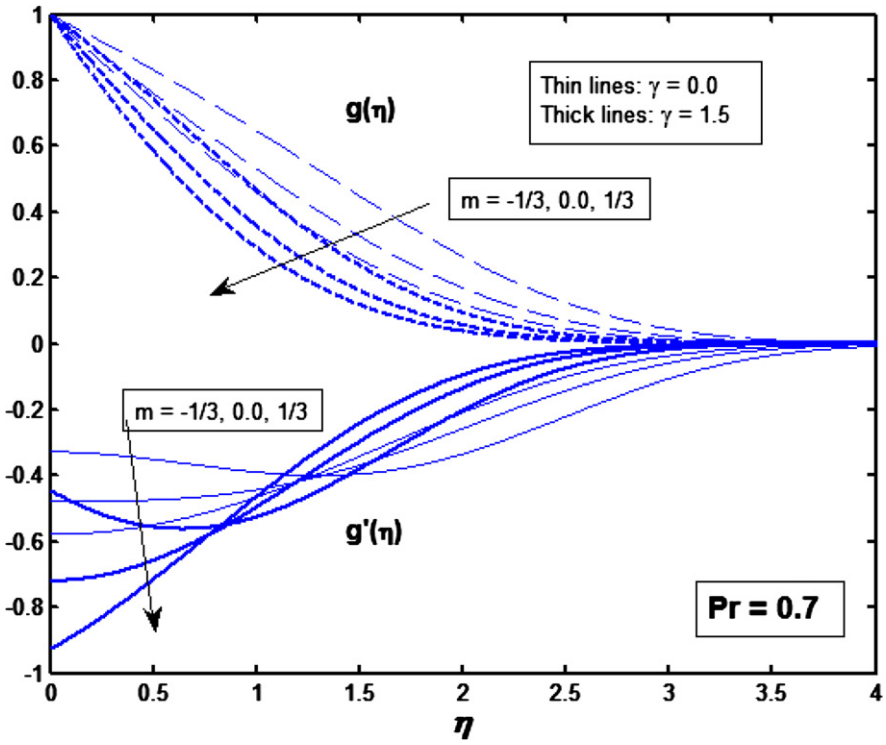

Fig. 7. The thermal boundary layer profiles for different m and γ with $Pr = 0.7$ for the upper branch solution.

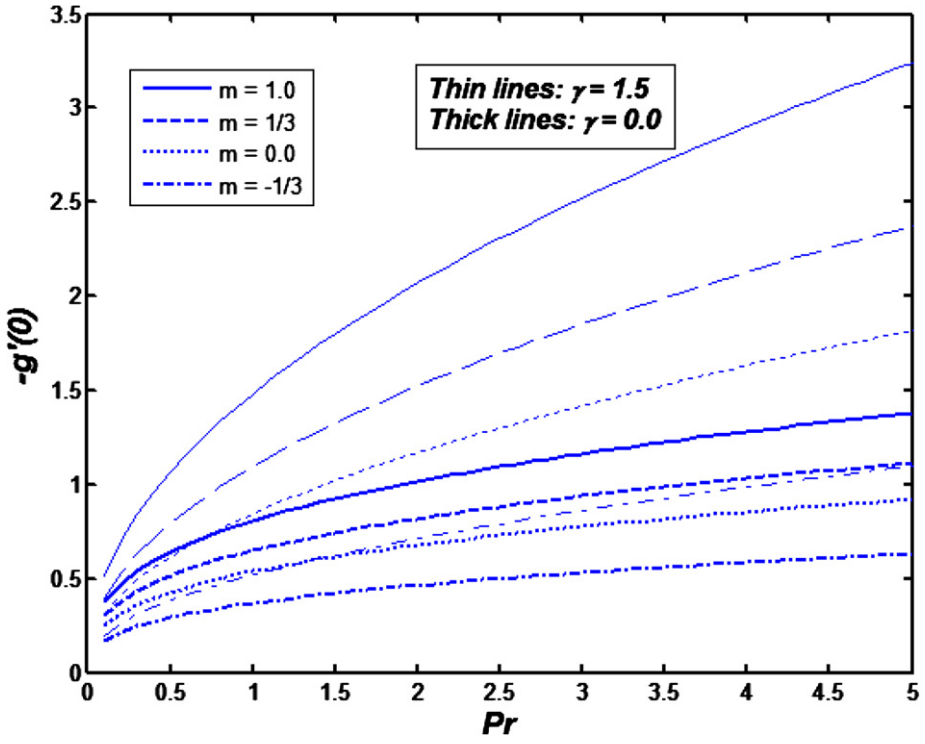

Fig. 8. The relationship of $-g'(0)$ to Pr for different m and γ for the upper solution branch.

the fluids not on the wall. The influence of the Prandtl number on the wall heat flux is shown in Fig. 8. Results show that the wall heat flux increases with the increase of Pr, m, and γ. The effects of power index m on the wall heat fluxes are illustrated in Fig. 9 for different wall stretching parameters and Prandtl numbers. For positive wall stretching, wall heat fluxes are increasing with the increase of Pr, γ, and m for $m > -\frac{2}{3}$. For $m < -\frac{2}{3}$, the heat is transferred

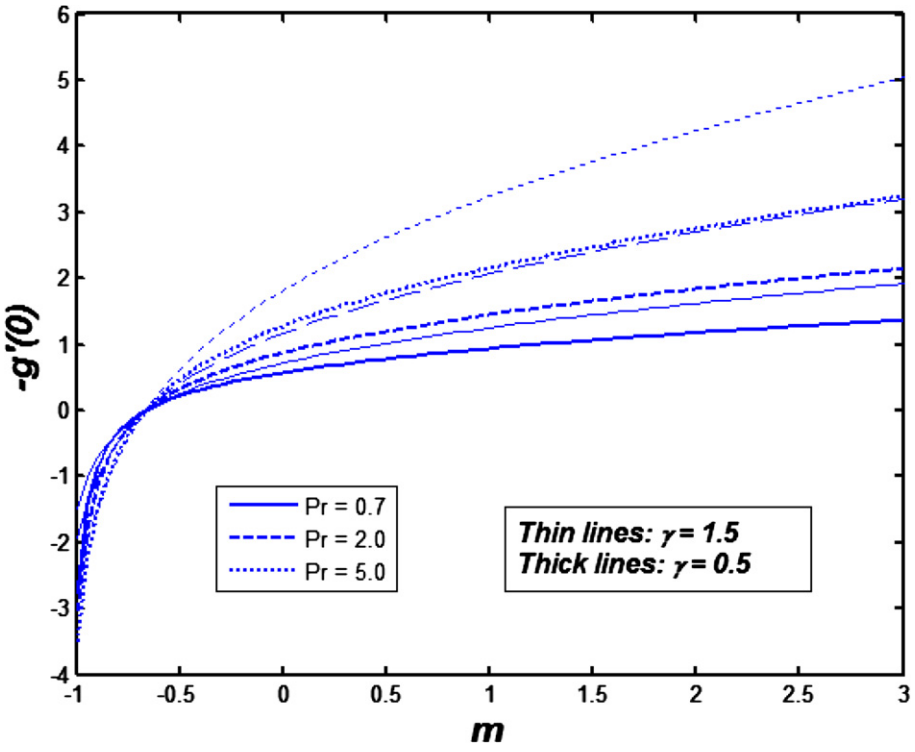

Fig. 9. The relationship of $-g'(0)$ to m for different Pr and positive γ of the upper solution branch.

from the fluid to the wall and the heat flux increases with increasing Pr and γ. From the results, it is expected that there is a certain value of m leading to an infinite heat flux and no finite solution for that m.

3.2.3.2. Solution for $\gamma < 0$. Examples of the thermal boundary layers for negative wall movement are illustrated in Fig. 10. For the upper solution branch, the thermal boundary layers are similar to those shown in Fig. 7. However,

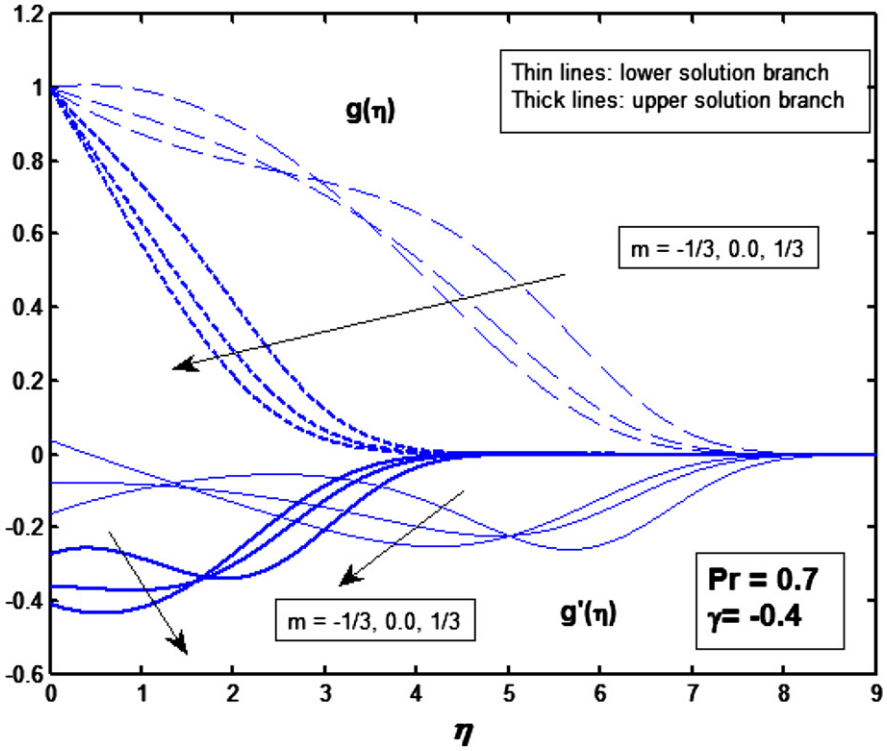

Fig. 10. The thermal boundary layer profiles for different m with $\gamma = -0.4$ and $Pr = 0.7$.

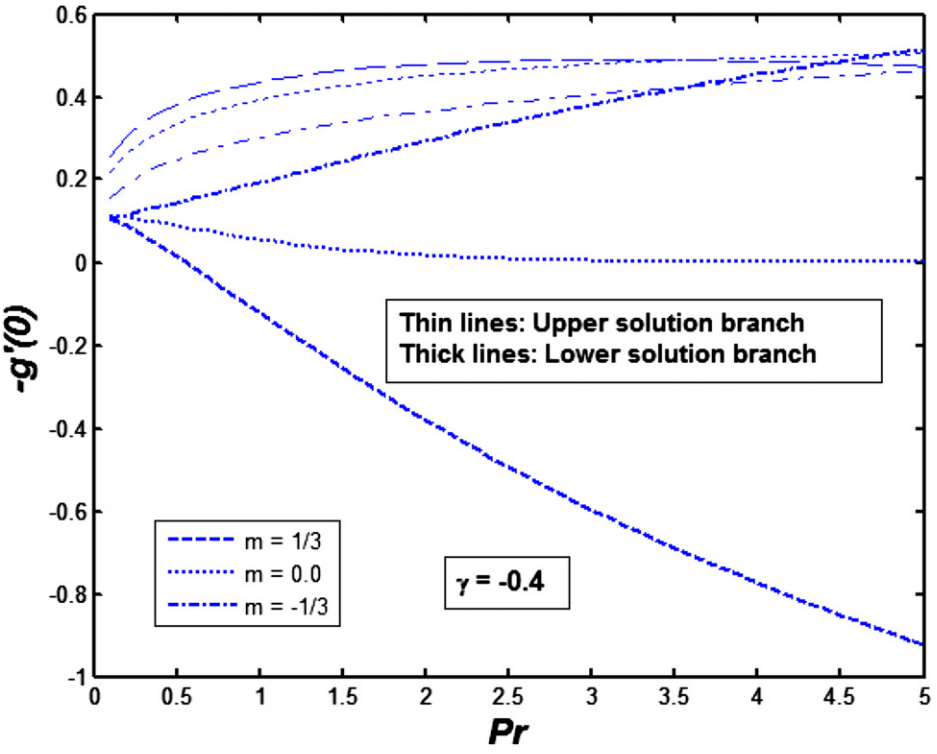

Fig. 11. The relationship of $-g'(0)$ to Pr for different with $\gamma = -0.4$.

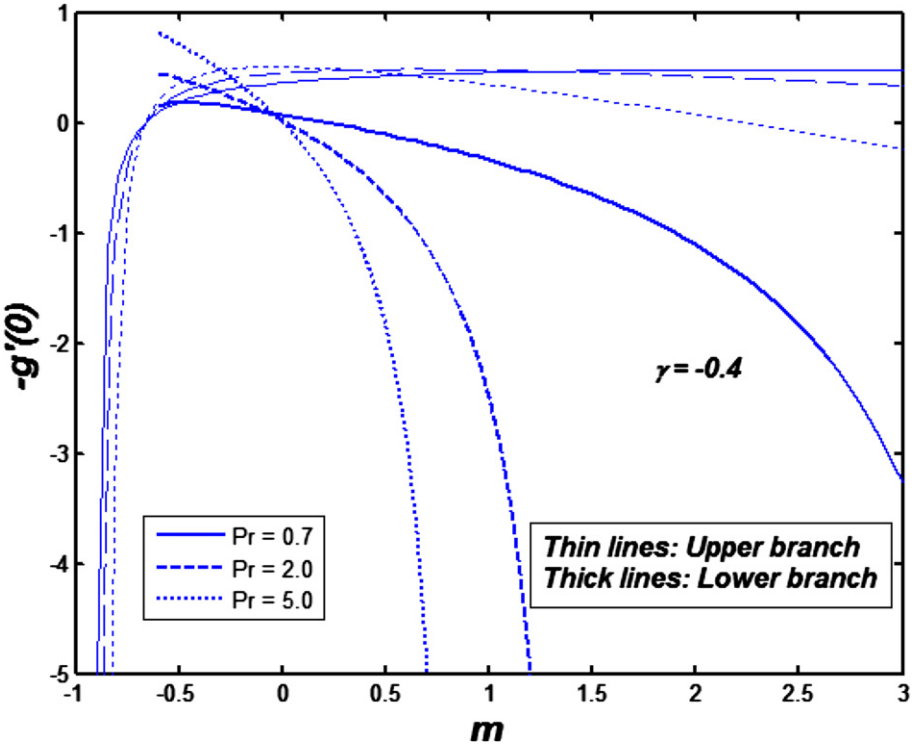

Fig. 12. The relationship of $-g'(0)$ to m for different Pr with $\gamma = -0.4$.

the temperature gradients generally have their extreme values in the fluid with a distance from the wall. The lower solution branch shows great different results. The boundary layer thickness is much thicker than the upper branch, and the thickness is increasing with the decrease of m. The temperature gradients at the wall are opposite to the upper

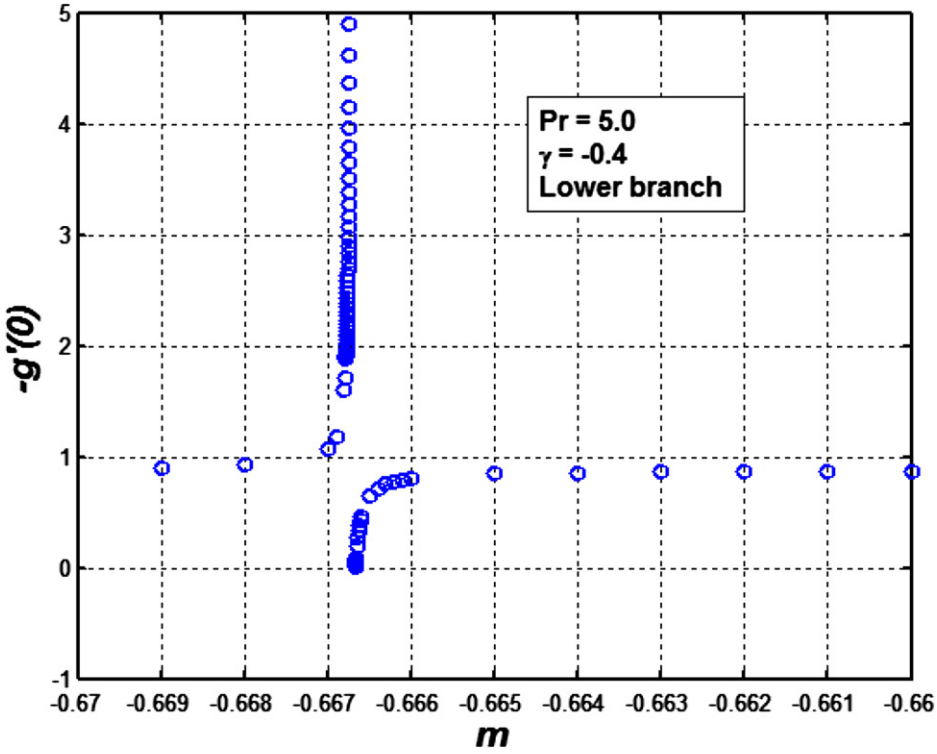

Fig. 13. The relationship of $-g'(0)$ to m when m is close to $-\frac{2}{3}$ for the lower solution branch with $Pr = 5.0$ and $\gamma = -0.4$.

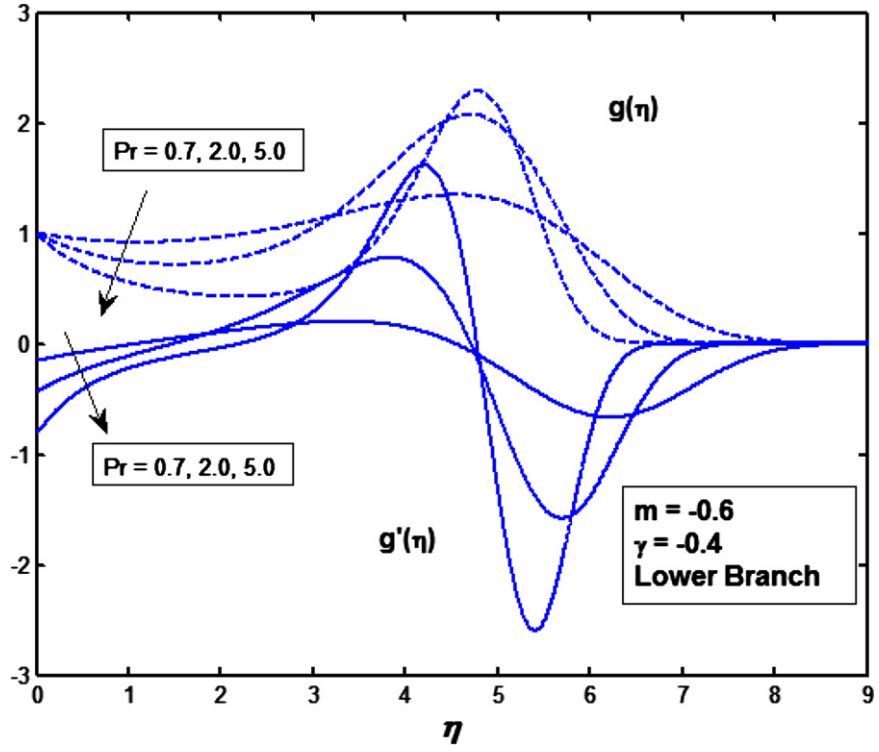

Fig. 14. The thermal boundary layer profiles for the lower solution branch of $\gamma = -0.4$ under different Pr with $m = -0.6$.

branch, and they are increasing with the decrease of m. For the lower branch, a positive temperature gradient occurs at the wall, in another word, the heat is transferred from the fluid to the wall. Without viscous dissipation, this seems not happen in a practical problem because the fluid temperature is less than the wall temperature. However, it is

possible for negative temperature power index m with positive wall stretching. Recalling the analytical solution for non-moving wall problem in Eqs. (29) and (30). It is shown that the wall becomes adiabatic for $m = -\frac{2}{3}$. There still exists solutions for Eq. (29) when $-1 < m < -\frac{2}{3}$. In this solution domain, the wall heat flux is negative with heat transferred from the fluid to the wall. The physical explanation is due to the negative power index. For negative power indices, the wall temperature decreases with the distance from the leading edge. The fluid temperature in the upstream has higher temperature than a location in the downstream. The heat from the upstream hotter fluid is transferred to the colder fluid and wall in the downstream. This can only explain the situation with no wall movement or positive wall movement because the fluid moves in the same direction as the wall moving direction. However, the results in Fig. 10 occur for a positive power index, i.e. $m = \frac{1}{3}$. The reason for this is due to the negative wall moving velocity. As a matter of fact, for a negative moving wall, with a positive m, the heat is transferred from the downstream hotter fluid to the upstream colder fluid and the wall. Here the "upstream" and "downstream" are defined based on the free stream flow direction. The wall heat fluxes become quite complicated when the parameters change. As seen in Fig. 11, for negative wall stretching and negative m, the wall heat fluxes does not necessarily increase with the increase of the Prandtl number. For the upper solution branch, the wall heat flux first increases and then drops down for certain m with the increase of the Prandtl numbers. For the lower solution branch, m plays an important role in affecting the wall heat flux. There are quite big differences for different values of m. For a negative m, the wall heat flux increases with the increase of Pr. However for a positive m, the wall heat flux changes its sign from wall-to-fluid to fluid-to-wall. For a large Pr, the heat flux from the fluid to the wall increases with increasing Pr.

The effects of power index m on the wall heat fluxes are shown in Fig. 12. For the upper branch, the temperature gradient first increases with m and then drops down and also changed the sign from positive to negative with m passing $-\frac{2}{3}$. There is an obvious limiting value of m for different Prandtl numbers leading to no finite solution. For the lower solution branch, the behaviors look quite different. The adiabatic wall seems not occur at $m = -\frac{2}{3}$. The heat flux drops from positive to negative and it is also obvious that there is a limiting m value making the solution infinite for a certain Prandtl number. With the increase of Pr, the limiting value becomes smaller. Based on the result of the lower branch in Fig. 12, it seems that the solution is not consistent with the analytical solution of Eq. (24) for $m = -\frac{2}{3}$. However, a further look at the solution near $m = -\frac{2}{3}$ shows interesting results. An example is shown in Fig. 13 for $Pr = 5.0$ and $\gamma = -0.4$ with the lower solution branch. From Fig. 13, when m is approaching $-\frac{2}{3}$ from the right, the solution becomes the same as the analytical solution from Eq. (24). $m = -\frac{2}{3}$ is a separating line. When m approaches $-\frac{2}{3}$ from the left-hand side, the solution becomes infinite when it is close enough to the vertical line. This shows that the thermal boundary layers of the lower

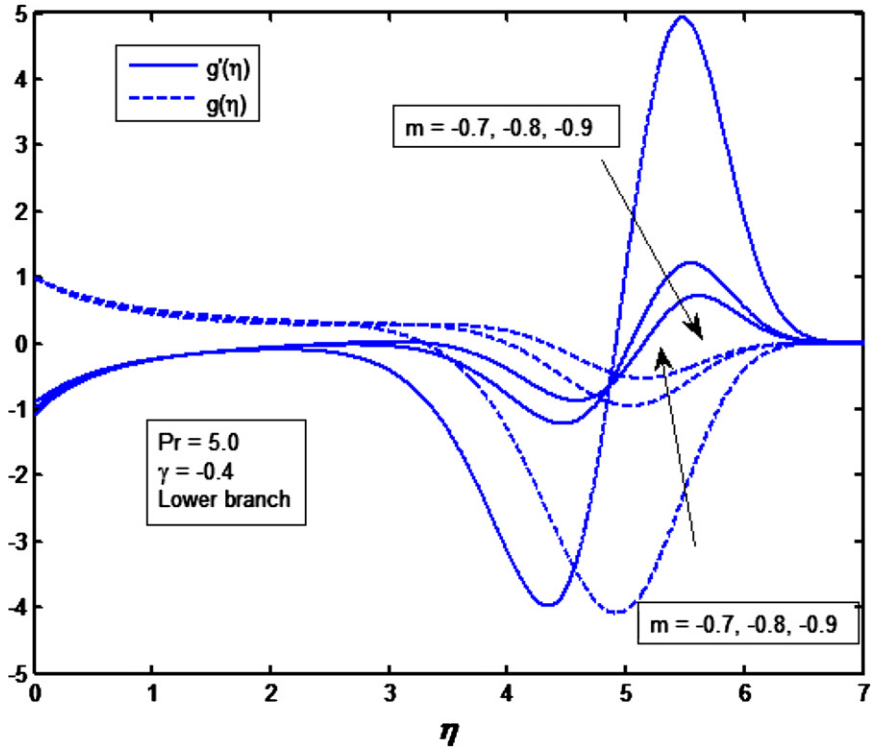

Fig. 15. The thermal boundary layer profiles for the lower solution branch of $\gamma = -0.4$ with $Pr = 5.0$ and $m = -0.7, -0.8, -0.9$.

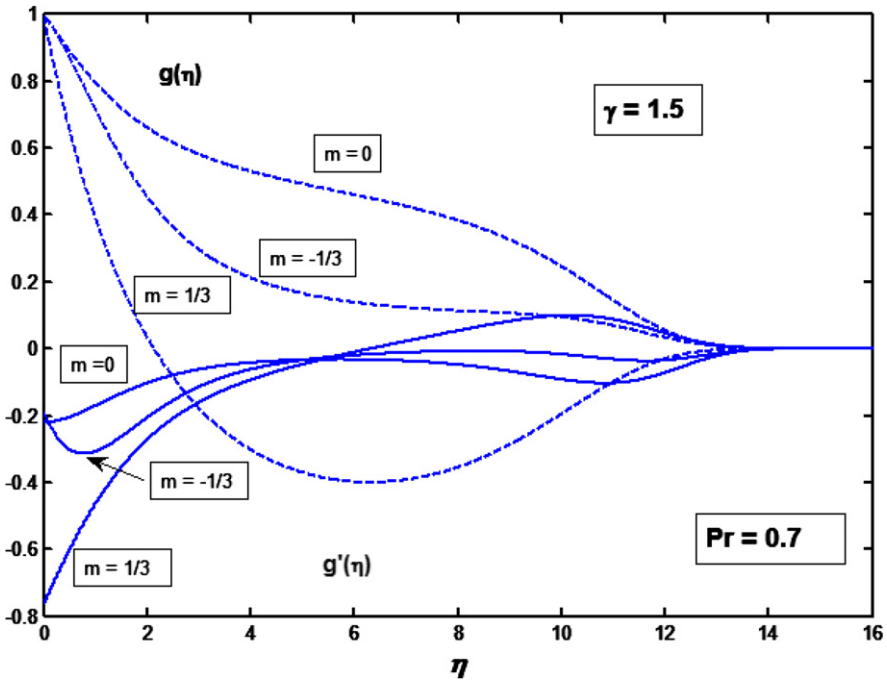

Fig. 16. The thermal boundary layer profiles for different m and $\gamma = 1.5$ with $Pr = 0.7$ for the lower branch solution.

solution branch are consistent with the analytical solution. However, the thermal boundary layer itself can have very complicated behaviors. Some examples are illustrated in Fig. 14 for $m = -0.6$ for different Prandtl numbers at $\gamma = -0.4$. With the increase of the distance from the wall, the fluid temperature first drops down, then increases, and then decreases again to the ambient temperature. Results from the solution to the left of $m = -\frac{2}{3}$ are shown in Fig. 15 for different values of m. There are negative temperatures in the boundary layers, which are not consistent with the physical configurations. These solutions only have mathematical meaning with no physical implementations. Generally speaking, the unphysical solution only occurs for certain negative temperature power and wall stretching values.

3.2.3.3. Lower solution branch for $\gamma > 0$. As seen in the momentum boundary layers in previous section, the lower solution branch shows quite interesting behaviors with reversal flow for positive stretching. Even though the physical implementation of such a flow is quite difficult, it is worthy of further investigation from the mathematical point of view. An example of the thermal boundary layers for different m and $\gamma = 1.5$ with $Pr = 0.7$ for the lower branch solution is shown in Fig. 16. The results for $m = 0$ and $m = -\frac{1}{3}$ are similar to the temperature profiles discussed above. However, for $m = \frac{1}{3}$, there is negative temperature occurring in the thermal boundary layer, which is not consistent with the physical configuration for the current problem. Generally speaking, the unphysical solution occurs under certain temperature power index and wall stretching parameters for the lower solution branch.

4. Conclusion

In this paper, the flow and heat transfer characteristics of the boundary layers over a continuously stretching surface with a uniform-shear free stream were investigated. Some findings can be summarized as follows:

1. Dual solutions exist for certain wall stretching parameters, namely $-0.596985 < \gamma_c$. There is only one solution for $\gamma_c = -0.596985$. There is no solution for $\gamma_c < -0.596985$.
2. With wall stretching, the free stream is no longer a Couette shear profiles. There is an induced free-stream velocity depending on the wall stretching parameter and solution branch.
3. Analytical solutions were presented for some special cases of thermal boundary layers with $m = -\frac{2}{3}$ and $m = 0$.
4. Exact analytical solutions of the thermal boundary layers for non-stretching shear problem, namely $\gamma = 0$, with arbitrary Pr and m was derived. The limiting conditions for large Pr and m were also solved analytically.
5. The thermal boundary layers are greatly affected by the Prandtl number, the temperature power exponent, and the wall stretching parameter. The variation trends are relatively simple for positive γ and m for the upper solution branch. However, for negative γ and m and the lower solution branch, the boundary layer flow becomes more interesting and difficult to predict.
6. The flow and heat transfer characteristics of the boundary layers over a stretching surface in the presence of a uniform-shear free stream are greatly different from

the boundary layers with rotation-free free-stream conditions.

Acknowledgements

The author expresses his sincere appreciation to the reviewers for their time and interests and constructive comments.

References

[1] T. Altan, S. Oh, H. Gegel, Metal Forming Fundamentals and Applications, American Society of Metals, Metals Park, OH, 1979.
[2] E.G. Fisher, Extrusion of Plastics, Wiley, New York, 1976.
[3] Z. Tadmor, I. Klein, Engineering principles of Plasticating Extrusion, Polymer Science and Engineering Series, Van Norstrand Reinhold, New York, 1970.
[4] B.C. Sakiadis, Boundary-layer behavior on continuous solid surface: I. Boundary-layer equations for two-dimensional and axisymmetric flow, J. AIChe. 7 (1961) 26–28.
[5] B.C. Sakiadis, Boundary-layer behavior on continuous solid surface: II. Boundary-layer on a continuous flat surface, J. AIChe 7 (1961) 221–225.
[6] F.K. Tsou, E.M. Sparrow, R.J. Goldstain, Flow and heat transfer in the boundary layer on a continuous moving surface, Int. J. Heat Mass Transfer 10 (1967) 219–235.
[7] L.J. Crane, Flow past a stretching plate, Z. Angew. Math. Phys. 21 (4) (1970) 645.
[8] B.K. Dutta, P. Roy, A.S. Gupta, Temperature field in flow over a stretching sheet with uniform heat flux, Int. Commun. Heat Mass Transfer 12 (1985) 89–94.
[9] L.J. Grubka, K.M. Bobba, Heat transfer characteristics of a continuous stretching surface with variable temperature, ASME J. Heat Transfer 107 (1985) 248–250.
[10] C.K. Chen, M.I. Char, Heat transfer of a continuous stretching surface with suction and blowing, J. Math. Anal. Appl. 135 (1988) 568–580.
[11] M.E. Ali, On thermal boundary layer on a power law stretched surface with suction or injection, Int. J. Heat Fluid Flow 16 (1995) 280–290.
[12] E.M.A. Elbashbeshy, Heat transfer over a stretching surface with variable surface heat flux, J. Phys. D: Appl. Phys. 31 (1998) 1951–1954.
[13] T.A. Abdelhafez, Skin friction and heat transfer on a continuous flat surface moving in a parallel free stream, Int. J. Heat Mass Transfer 28 (1985) 1234–1237.
[14] P.R. Chappidi, F.S. Gunnerson, Analysis of heat and momentum transport along a moving surface, Int. J. Heat Mass Transfer 32 (1989) 1383–1386.
[15] N. Afzal, A. Badaruddin, A.A. Elgarvi, Momentum and heat transport on a continuous flat surface moving in a parallel stream, Int. J. Heat Mass Transfer 36 (13) (1993) 3399–3403.
[16] C.Y. Wang, The boundary layers due to shear flow over a still fluid, Phys. Fluids A 4 (6) (1992) 1304–1306.
[17] P.D. Weidman, D.G. Kubitschek, Boundary layer similarity flow driven by power-law shear, Acta Mechan. 120 (1–4) (1997) 199–215.
[18] E. Magyari, B. Keller, I. Pop, Boundary-layer similarity flows driven by a power-law shear over a permeable plane surface, Acta Mechan. 163 (3–4) (2003) 139–146.
[19] G.E. Cossali, Similarity solutions of energy and momentum boundary layer equations for a power-law shear driven flow over a semi-infinite flat plate, Eur. J. Mech. B Fluid. 25 (1) (2006) 18–32.
[20] M. Guedda, A note on boundary-layer similarity flows driven by a power-law shear over a plane surface, Fluid Dyn. Res. (2007), doi:10.1016/j.fluiddyn.2006.11.005.
[21] G.E. Cossali, Power series solutions of momentum and energy boundary layer equations for a power-law shear driven flow over a semi-infinite flat plate, Int. J. Heat Mass Transfer 49 (21–22) (2006) 3977–3983.
[22] E. Magyari, B. Keller, I. Pop, Heat transfer characteristics of a boundary-layer flow driven by a power-law shear over a semi-infinite flat plate, Int. J. Heat Mass Transfer 47 (1) (2004) 31–34.
[23] E. Magyari, P.D. Weidman, Thermal characteristics of the Airy wall jet for constant surface heat flux, Heat Mass Transfer 42 (9) (2006) 813–816.
[24] E. Magyari, P.D. Weidman, The preheated Airy wall jet, Heat Mass Transfer 41 (11) (2005) 1014–1020.
[25] E. Magyari, P.D. Weidman, Heat transfer on a plate beneath an external uniform shear flow, Int. J. Therm. Sci. 45 (2) (2006) 110–115.
[26] C.Y. Wang, Shear flow over a wall with variable temperature, ASME Trans. J. Heat Transfer 113 (1991) 496–498.
[27] F.M. White, Viscous Fluid Flow, second ed., McGraw-Hill, New York, 1991.
[28] S. Goldstein, On backward boundary layers and flow in converging passages, J. Fluid Mech. 21 (1965) 33–45.
[29] J.P. Klemp, A. Acrivos, A moving-wall boundary layer with reverse flow, J. Fluid Mech. 53 (1) (1972) 177–191.
[30] K. Vajravelu, R.N. Mohapatra, On fluid dynamic drag reduction in some boundary layer flows, Acta Mechan. 81 (1990) 59–68.
[31] T. Fang, Further study on a moving-wall boundary-layer problem with mass transfer, Acta Mechan. 163 (3–4) (2003) 183–188.
[32] M.Y. Hussaini, W.D. Lakin, A. Nachman, On similarity solution of a boundary layer problem with upstream moving wall, SIAM J. Appl. Math. 7 (4) (1987) 699–709.
[33] S. Wolfram, Mathematica – A System for Doing Mathematics by Computer, second ed., Addison-Wesley Publishing Company, Inc., New York, 1993.